Enhanced energy transfer in Nd^{3+}/Cr^{3+} co-doped $Ca_3Ga_2Ge_3O_{12}$ phosphors with near-infrared and long-lasting luminescence properties

Huihong Lin, [a,b] Ting Yu, [b] Gongxun Bai, [a,c] Ming-Kiu Tsang, [a,c] Qinyuan Zhang, [b] Jianhua Hao [a,c*]

The phosphors of $Ca_3Ga_2Ge_3O_{12}$(CGGG) co-doped with Nd^{3+} and Cr^{3+} ions were synthesized by conventional solid-state reaction technique. Steady-state and time-resolved near-infrared (NIR) photoluminescence (PL) and long-lasting phosphorescence (LLP) properties are investigated in the Nd^{3+}-doped CGGG samples. An increase in NIR luminescence traps can be realized in Nd^{3+}/Cr^{3+} co-doped samples. Energy transfer from Cr^{3+} to Nd^{3+} with the efficiency up to 57.5 % is evident for the $Ca_{3-x}Nd_xGa_{1.99}Cr_{0.01}Ge_3O_{12}$ at x = 0.09. A cross relaxation scheme related to $^4T_2$-$^4A_2$ of Cr^{3+} and $^4I_{9/2}$-$^4F_{3/2}$ transition of Nd^{3+} is discussed. We have present the luminescence mechanism involving the competing processes of NIR PL and LLP, which accords with our measurements. The results show that the NIR persistent luminescence of CGGG co-doped with Nd^{3+} and Cr^{3+} is more efficient compared to the single Nd^{3+} ion doped CGGG.

Introduction

Persistent luminescence materials relate to a particular optical phenomenon in which the excitation energy can be stored by the material and then slowly released by the form of photon emission, capable of lasting up to long hours.[1] In persistent phosphors, two kinds of functional centers are involved, namely emitter and trap. Emitters are the centers capable of emitting radiation after being excited. Traps usually do not emit radiation by themselves, instead they store excitation energy which can be gradually released and transferred to the emitters owing to thermal or other physical stimulations. Near-infrared (NIR) luminescence (ca. 700-2500 nm) makes compelling using in many technologically important applications, including optical telecommunication, spectral conversion for solar energy, or in biomedical optical imaging.[2,3] NIR long-lasting phosphorescence (LLP) phosphors have attracted enormous attention in recent years, which shows the potential as optical probes in some research fields, such as biomedical imaging.[4-6] In such phosphors, a suitable emitter is required to emit NIR light while a proper host is needed to create appropriate traps and therefore promote persistent luminescence.

For NIR LLP photoluminescence, trivalent chromium (Cr^{3+}), is a favorable luminescent centre in solids because of its narrow-band emissions (usually near 700 nm) due to the spin forbidden $^2E \rightarrow ^4A_2$ transition, or a broadband emission (650-1600 nm) due to the spin-allowed $^4T_2 \rightarrow ^4A_2$ transition, which strongly depends on the crystal-field environment of the host lattices. Cr^{3+}-doped NIR LLP luminescence materials can be found from some reports, such as $Zn_3Ga_2Ge_2O_{10}$:Cr^{3+} (λ_{em} = 696 nm), $Zn(Ga_{1-x}Al_x)_2O_4$: Cr^{3+},Bi^{3+} (λ_{em} = 696 nm), $ZnGa_2O_4$:Cr^{3+}(λ_{em} = 696 nm), $La_3Ga_5GeO_{14}$: Cr^{3+} (λ_{em} = 688, 1000 nm), $LiGa_5O_8$:Cr^{3+}(λ_{em} = 716 nm), and CGGG: Cr^{3+} (λ_{em} = 750 nm).[7-15] According to recent optical coherence tomography studies, the NIR wavelength ranging from 800 to 1300 nm is useful for high-resolution imaging because of its lowest amount of light loss through scattering.[16,17] The demand for inorganic phosphors exhibiting longer NIR wavelengths has been growing for the use in high-resolution *in vivo* imaging.

On the other hand, the electron configuration of Nd^{3+} ion is [Xe]$4f^3$. The energy level structure of Nd^{3+} shows a multitude of levels, many of which are emissive in nature. Specially, typical electron transition from the excited state $^4F_{3/2}$ to the ground state $^4I_{11/2}$ corresponds to the emission at the wavelength of around 1064 nm, which satisfies fairly well the requirements of *in vivo* optical imaging.[18] Recently, the NIR LLP luminescence has been found in aluminate phosphors doped with Nd^{3+}, such as $SrAl_2O_4$:Eu^{2+}, Dy^{3+}, Nd^{3+} (λ_{em} = 882 and 1064 nm), and $CaAl_2O_4$:Eu^{2+}, Nd^{3+} (λ_{em} = 880 and 1060 nm), through the energy transfer process from the excited Eu^{2+} ions to Nd^{3+} ions.[19,20]

Nd^{3+}:CGGG crystal is a solid-state laser material, which shows good spectroscopic properties for infrared laser oscillation.[21] According to our current experiments, Nd^{3+}: CGGG might involve NIR (λ_{em} = 886, 940 and 1062nm) LLP luminescent properties. Because Cr^{3+} based LLP emission in CGGG falls into the wavelength range of 700-900 nm (peaking at about 750 nm),[10,15] it can be a perfect overlap with the excitation spectrum of Nd^{3+} in the same host. Motivated by the two interests, namely one is to broaden the NIR LLP spectral range from 700 to 1300 nm, and the other is to enhance Nd^{3+} NIR LLP luminescence, we design and synthesize a series of Nd^{3+} and Cr^{3+} co-doped CGGG phosphors. In this work, the investigation on NIR downshifting (DS) and LLP luminescence are presented

a. Department of Applied Physics, The Hong Kong Polytechnic University, Hong Kong, P. R. China.
b. State Key Laboratory of Luminescence Materials and Devices, and Institute of Optical Communication Materials, South China University of Technology, Guangzhou 510641, P. R. China
c. The Hong Kong Polytechnic University Shenzhen Research Institute, Shenzhen 518057, P.R. China
* E-mail: jh.hao@polyu.edu.hk.

in CGGG: Nd^{3+} and CGGG: Nd^{3+}, Cr^{3+} phosphors. More importantly, the energy transfer mechanisms from Cr^{3+} to Nd^{3+} are discussed. In particular, the energy transfer efficiency is greatly enhanced by increasing the traps of NIR persistent luminescence with co-doped Cr^{3+} into Nd^{3+}: CGGG.

Experimental

A series of powder samples were synthesized by a solid state reaction technique at high temperature. The reactants include 99.99% $CaCO_3$, 99.999% Ga_2O_3, 99.999% GeO_2, 99.95% Cr_2O_3, and 99.99% Nd_2O_3. According to the nominal compositions of compounds $Ca_{3-x}Nd_xGa_2Ge_3O_{12}$, $Ca_{3-x}Nd_xGa_{1.99}Cr_{0.01}Ge_3O_{12}$ (x = 0, 0.01, 0.03, 0.09, 0.15), and $Ca_{2.97}Nd_{0.03}Ga_{2-x}Cr_xGe_3O_{12}$ (x = 0.005, 0.01, 0.03, 0.05, 0.07), appropriate amount of starting materials was thoroughly mixed and ground, and subsequently the mixture was prefired at 900 °C for 2 h. After slowly cooling down to room temperature, the prefired samples were thoroughly reground and then calcined at 1200 °C for 6 h in air atmosphere. The products were cooled down slowly to room temperature (RT) by switching off the muffle furnace and finally ground into white powder.

Phase identification of the obtained products was analyzed by means of a Philips PW1830 X-ray powder diffractometer (XRD) using graphite monochromator and Cu Kα (λ = 1.54056Å) radiation at 40 kV and 40 mA. Diffuse reflectance spectra (DRS) were recorded using a Cary 5000 UV-VIS-NIR spectrophotometer equipped with a double out-of-plane Littrow monochromator using $BaSO_4$ as a standard reference. Steady-state photoluminescence (PL) spectra were determined using an Edinburgh FLS920 spectrofluorimeter equipped with continuous wave 450 W xenon lamp excitation source, liquid-nitrogen cooled R5509-72 NIR PMT for photon detection. Besides, dynamic fluorescence spectra like decay curves were recorded with microsecond μF900 xenon lamp excitation sources. DS emission spectra were recorded on the Jobin-Yvon TRIAX320 spectrofluorimeter equipped with a R928 photomultiplier tube as the detector and a 808 nm laser diode (LD, Coherent Corp.) as monochromatic light source. Thermoluminescence (TL) glow curves were measured with a FJ-427A TL meter (Beijing Nuclear Instrument Factory) by heating the irradiated samples from 313 to 473 K. The samples were pre-irradiated by using a 254 Xe lamp for 5 min and then heated at a linear rate of 2 K s⁻¹ to release the energy reserved in the material. Limited by the measuring system, the test can't be performed for detecting NIR LLP spectra or decay curves at this stage. All the PL spectra were corrected for the wavelength-dependent response of the detector system. For comparison, the spectra were recorded under identical measurement conditions. Appropriate optical filters were used to avoid stray light in all spectral measurements. All measurements were carried out at room temperature.

Results and discussion

Structure and phase characterizations

Fig. 1a shows the XRD patterns of the CGGG standard card (JCPDS 11-0023) and the samples $Ca_3Ga_{1.99}Cr_{0.01}Ge_3O_{12}$, $Ca_{2.97}Nd_{0.03}Ga_2Ge_3O_{12}$, and $Ca_{2.97}Nd_{0.03}Ga_{1.99}Cr_{0.01}Ge_3O_{12}$, labeled as curves 1, 2, 3, and 4, respectively. It can be observed that curves 2, 3, 4 are in good agreement with curve 1. This suggests that the substitutions of Ca^{2+} by Nd^{3+} or Ga^{3+} by Cr^{3+} have little influence on the host crystal structure. It was reported that the crystal structure of CGGG is cubic garnet-type structure with space group *Ia-3d*.[10] The Ca^{2+}, Ga^{3+}, and Ge^{4+} cations are surrounded by eight, six, and four oxygen anions forming a dodecahedron, an octahedron, and a tetrahedron respectively, as displayed in Fig. 1 b. The approximate ionic radii of Ca^{2+}, Ga^{3+}, and Ge^{4+} cations in CGGG are as follows: Ca on dodecahedral site (CN = 8, r = 1.12 Å); Ga on octahedral site (CN = 6, r = 0.62 Å); Ge on tetrahedral site (CN = 4, r = 0.53 Å). Here, it is noted that the doped rare-earth Nd^{3+} ion enters the dodecahedral site of Ca^{2+}, while transition metal Cr^{3+} ion easily enters the octahedral site of Ga^{3+} in the CGGG host due to their similar ionic radii.

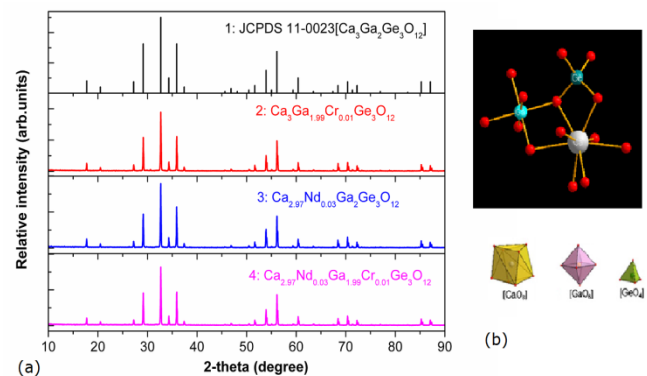Fig. 1. (a) XRD patterns of the samples $Ca_3Ga_{1.99}Cr_{0.01}Ge_3O_{12}$, $Ca_{2.97}Nd_{0.03}Ga_2Ge_3O_{12}$, and $Ca_{2.97}Nd_{0.03}Ga_{1.99}Cr_{0.01}Ge_3O_{12}$. (b) Schematic diagram of $Ca_3Ga_2Ge_3O_{12}$ structure and coordination environment of the Ca^{2+}, Ga^{3+}, and Ge^{4+} cations.

Diffuse Reflectance Spectra (DRS)

The diffuse reflectance spectra of samples $Ca_3Ga_2Ge_3O_{12}$, $Ca_3Ga_{1.99}Cr_{0.01}Ge_3O_{12}$, $Ca_{2.97}Nd_{0.03}Ga_2Ge_3O_{12}$, and $Ca_{2.97}Nd_{0.03}Ga_{1.99}Cr_{0.01}Ge_3O_{12}$ are displayed in Fig. 2. The powders are transparent in the visible region and show an increased absorption when the wavelength approaches towards 200 nm. With the method by Kumar et al.,[22] as shown in the inset of Fig. 2, the estimated band gap of CGGG host is 5.5 eV (~225 nm, 44.444 cm⁻¹). Other three curves correspond to the respective absorptions of the doped samples $Ca_3Ga_{1.99}Cr_{0.01}Ge_3O_{12}$, $Ca_{2.97}Nd_{0.03}Ga_2Ge_3O_{12}$, and $Ca_{2.97}Nd_{0.03}Ga_{1.99}Cr_{0.01}Ge_3O_{12}$. The result of undoped CGGG host is also listed for comparison.
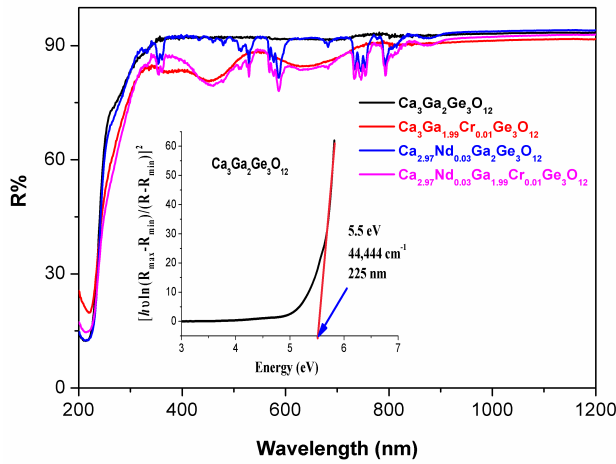
Fig. 2. The diffuse reflection spectra of $Ca_3Ga_2Ge_3O_{12}$, $Ca_3Ga_{1.99}Cr_{0.01}Ge_3O_{12}$, $Ca_{2.97}Nd_{0.03}Ga_2Ge_3O_{12}$, and $Ca_{2.97}Nd_{0.03}Ga_{1.99}Cr_{0.01}Ge_3O_{12}$. The inset shows a plot for CGGG of $[hv\ln\{(R_{max} - R_{min})/(R - R_{min})\}]^2$ against energy (eV), where R is reflectance, to estimate the band gap.

The NIR-to-NIR DS and NIR persistence luminescence of Nd^{3+} in $Ca_3Ga_2Ge_3O_{12}$.

Fig. 3a shows the NIR excitation and emission spectra of the sample $Ca_{2.97}Nd_{0.03}Ga_2Ge_3O_{12}$ at the optimal concentration for Nd^{3+}. Under 1062 nm NIR light monitoring, the excitation spectrum shows several sharp lines peaked at about 354, 469, 527, 584, 690, 746, and 806 nm, due to $^4I_{9/2}$ to $^4D_{1/2}(^4D_{3/2})$, $^4G_{9/2}$, $^2K_{13/2}(^4G_{7/2})$, $^4G_{5/2}(^2G_{7/2})$, $^4F_{9/2}$, $^4S_{3/2}(^4F_{7/2})$, and $^4F_{5/2}(^2H_{9/2})$ transitions, respectively. In addition, an incomplete broad band peaked at ~220 nm can be observed in excitation spectrum, which is probably attributed to the fundamental absorption edge of the host material CGGG (~225 nm from Fig. 2).[24] From the excitation spectrum, we can draw a conclusion that there are strong absorptions near the wavelength of 800 nm in single Nd^{3+} activated CGGG phosphors. In the NIR Stokes emission spectrum, it can be observed that three peaks located at 890, 1062, and 1350 nm, which are ascribed to the electron transition in Nd^{3+} ions from the excited state $^4F_{3/2}$ to the ground state ^4I_J (J = 9/2, 11/2, 13/2) upon 808 nm NIR light (Xe lamp) excitation. The transition from $^4F_{3/2}$ to $^4I_{11/2}$ (~ 1062 nm) is dominant among these emission intensities.

Fig. 3b shows the decay curve at 1062 nm for the sample $Ca_{2.97}Nd_{0.03}Ga_2Ge_3O_{12}$ emission under the excitation at 808 nm. The curve can be well fitted by a bi-exponential equation,[23]

$$I_t = I_0 + A_1 \exp(-t/\tau_1) + A_2 \exp(-t/\tau_2) \tag{1}$$

where I is the luminescence intensity, A_1 and A_2 are characteristic constants, t is the time, and τ_1 and τ_2 are the decay times for the bi-exponential components, respectively. The values of τ_1 and τ_2 are calculated from the fitted curves, as shown in Fig. 3(b). The decays of $^4F_{3/2}$ are non-monoexponential, due to the energy transfer mechanism by cross relaxation among Nd^{3+} energy levels, which occurs frequently at relatively high concentration with 1% mol. According to the energy level of Nd^{3+}, as displayed later, possible cross-relaxation process is as follows: $^4F_{3/2} + {}^4F_{3/2} \rightarrow {}^4I_{11/2} + {}^2G_{9/2}$ and $^4F_{3/2} + {}^4F_{3/2} \rightarrow {}^4I_{13/2} + {}^4G_{7/2}$.
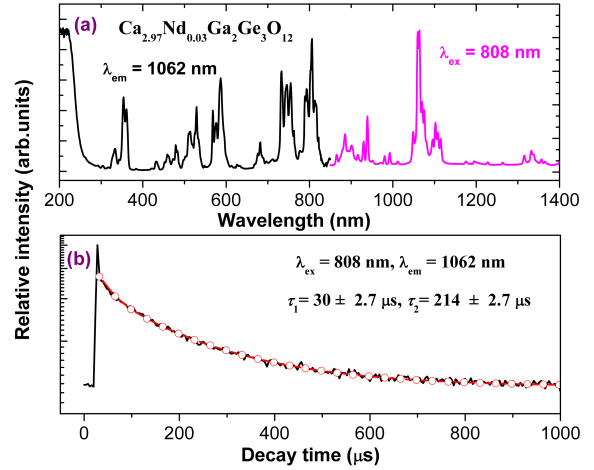

Fig. 3. (a) The excitation and emission spectra of the sample $Ca_{2.97}Nd_{0.03}Ga_2Ge_3O_{12}$. (b) The decay and fitted curves of $Ca_{2.97}Nd_{0.03}Ga_2Ge_3O_{12}$ upon 808 nm excitation with 1062 nm emission wavelength.

TL curves were measured from the $Ca_{3-x}Nd_xGa_2Ge_3O_{12}$ samples excited by 254 nm source for 5 min. As an example, the sample with x = 0.03 is shown in Figure 4. As revealed in Fig. 4, a typical broadband composed of two peaks is appeared in the TL curve measured from Nd: CGGG. The curve can be fitted well with a sum of two Gaussian profiles, marked as I (~ 79 °C) and II (~154 °C), corresponding to the shallow and deep traps, respectively. The thermal activation energy E of trapped carriers, which corresponds to the trap depth, can be estimated by Hoogenstraaten method. According to the fomula, $E = 2kT_m^2/\delta$, the values of E are 0.75 eV (peak I) and 1.15 eV (peak II) are obtained. [24,25]
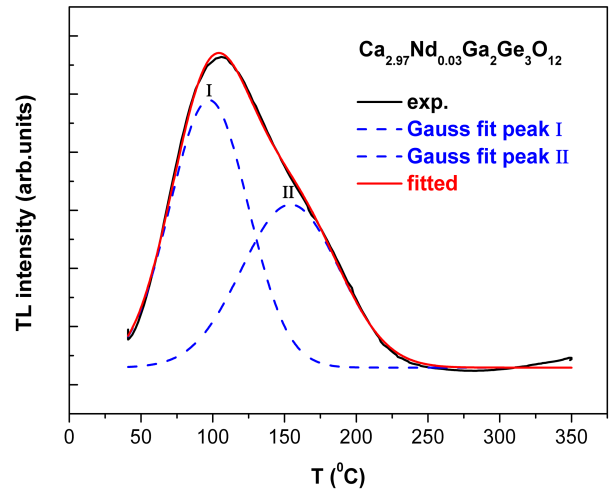

Fig. 4. TL curves of the samples $Ca_{3-x}Nd_xGa_2Ge_3O_{12}$ (x = 0.03) after 254 nm excitation for 5 min. The Gauss fit peaks of I and II are also shown.

The energy transfer mechanisms from Cr^{3+} to Nd^{3+} in $Ca_3Ga_2Ge_3O_{12}$.

Fig. 5a shows the photoluminescence excitation (PLE) spectrum at λ_{em} = 750 nm and PL spectrum at λ_{ex} = 267 nm of $Ca_3Ga_{1.99}Cr_{0.01}Ge_3O_{12}$. Here, one can observe three broad-bands peaked at about 247, 460, and 640 nm, along with a shoulder peak at ~310 nm in the excitation spectrum, attributed to the absorption of the CGGG host, the $^4A_2 \rightarrow {}^4T_1(^4F)$,

$^4A_2 \rightarrow ^4T_2(^4F)$, and $^4A_2 \rightarrow ^4T_1(^4P)$ transitions of Cr^{3+}, respectively. A broadband NIR emission (peak position at ~750 nm) appears in emission spectrum, which is ascribed to $^4T_2$-$^4A_2$ transition of Cr^{3+}. These results are consistent with the previous reports.[10,15]
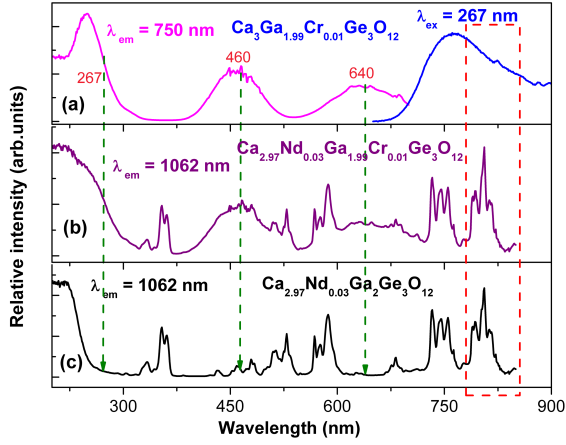

Fig. 5. (a) The excitation (λ_{em} = 750 nm) and emission (λ_{ex} = 267 nm) spectra of $Ca_3Ga_{1.99}Cr_{0.01}Ge_3O_{12}$. (b) The excitation spectrum of $Ca_{2.97}Nd_{0.03}Ga_{1.99}Cr_{0.01}Ge_3O_{12}$ under 1062 nm emission. (c) The excitation spectrum of $Ca_{2.97}Nd_{0.03}Ga_2Ge_3O_{12}$ under 1062 nm emission.

Fig. 5c illustrates the PLE spectrum of $Ca_{2.97}Nd_{0.03}Ga_2Ge_3O_{12}$ under 1062 nm emission, which is exactly same with that shown in Fig. 3a. When co-doping Cr^{3+} into the sample of $Ca_{2.97}Nd_{0.03}Ga_2Ge_3O_{12}$, for example $Ca_{2.97}Nd_{0.03}Ga_{1.99}Cr_{0.01}Ge_3O_{12}$, the excitation spectrum under 1062 nm emission is shown in Fig. 5b. It can be observed that obvious Cr^{3+} transitions are occurred except for Nd^{3+} absorptions. Therefore, energy transfer from Cr^{3+} to Nd^{3+} is evident. From Fig. 5, spectral overlap between the emission of Cr^{3+} and the excitation of Nd^{3+}, specifically close to 808 nm, is very efficient. It demonstrates that the NIR absorption of Nd^{3+} can be enhanced by incorporating Cr^{3+} into CGGG host.
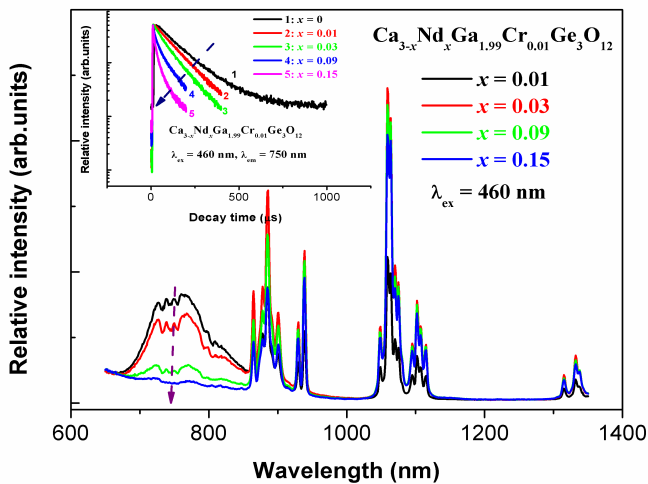

Fig. 6. The NIR DS emission spectra of the samples $Ca_{3-x}Nd_xGa_{1.99}Cr_{0.01}Ge_3O_{12}$ (x = 0.01, 0.03, 0.09, 0.15) upon 460 nm excitation. The inset shows the decay curves of the samples $Ca_{3-x}Nd_xGa_{1.99}Cr_{0.01}Ge_3O_{12}$ (x = 0, 0.01, 0.03, 0.09, 0.15) under the conditions of λ_{ex} = 460 nm, λ_{em} = 750 nm.

For further investigation, a series of $Ca_{3-x}Nd_xGa_{1.99}Cr_{0.01}Ge_3O_{12}$ (x = 0, 0.01, 0.03, 0.09, 0.15) samples with different doping concentrations of Nd^{3+} were synthesized. The NIR DS emission spectra of the samples upon 460 nm excitation are shown in Fig. 6. It is found that Cr^{3+} emission decreases by increasing the Nd^{3+} concentration, showing that the energy transfer results in the quenching of Cr^{3+} emission.

The energy transfer from Cr^{3+} to Nd^{3+} is investigated from the decay of the Cr^{3+} and Nd^{3+} emissions in co-doped $Ca_{3-x}Nd_xGa_{1.99}Cr_{0.01}Ge_3O_{12}$ samples. The inset of Figure 6 shows the decay times in the co-doped samples excited at 460 nm as a function of Nd^{3+} concentration for the Cr^{3+} emission at 750 nm. The decay times of Cr^{3+} decrease when increasing the Nd^{3+} concentration. When x = 0, i.e. $Ca_3Ga_{1.99}Cr_{0.01}Ge_3O_{12}$, after subtraction of the excitation pulse, the decay is fitted to the mono-exponential function with τ_0 = 134 μs. By combining with Fig. 6, it implies that the efficiency of energy-transfer from Cr^{3+} to Nd^{3+} is enhanced with the increase in Nd^{3+} concentration. The mono-exponential decay of Cr^{3+} in the presence of different Nd^{3+} concentrations indicates fast migration between donors so that the average acceptor distance is sensed by the donors.

The energy transfer efficiencies (η) for Cr^{3+} to Nd^{3+} transfer are calculated from the formula:

$$\eta = 1 - (\tau / \tau_0) \times 100\% \qquad (2)$$

where τ and τ_0 are the Cr^{3+} decay lifetime with and without the presence of Nd^{3+}, respectively. The energy transfer efficiency (η) increases with the increase of x value, listed in Table 1. The energy transfer from Cr^{3+} to Nd^{3+} takes place with the energy-transfer efficiency up to 57.5 % for the $Ca_{3-x}Nd_xGa_{1.99}Cr_{0.01}Ge_3O_{12}$ with x = 0.09.

Table 1. The energy transfer efficiencies (η) from Cr^{3+} to Nd^{3+} in samples $Ca_{3-x}Nd_xGa_{1.99}Cr_{0.01}Ge_3O_{12}$

x	0.01	0.03	0.09
τ (μs)	98	72	57
η	26.9%	46.3%	57.5%

The Nd^{3+} emission decay curves are also recorded for the series of $Ca_{3-x}Nd_xGa_{1.99}Cr_{0.01}Ge_3O_{12}$ (x = 0.01, 0.03, 0.09, 0.15) by exciting at 354 nm [$^4I_{9/2} \rightarrow ^4D_{1/2}(^4D_{3/2})$ transition of Nd^{3+}] and 640 nm [$^4A_2 \rightarrow ^4T_2(^4F)$ transition of Cr^{3+}] and monitoring the emission at 1062 nm, as shown in Fig. 7 a and b, respectively. It is also found that the decay lifetime of Nd^{3+} decreases by increasing the Nd^{3+} contents because of the increased the energy-transfer efficiency. For the sample with x = 0.01, a build-up trend is obviously observed in the beginning of the decay curve when exciting at 640 nm. The expected relatively slow decay upon excitation at 640 nm compared with that at 354 nm is attributed to the following reason. Nd^{3+} possesses $4f$ - $4f$ absorption bands at 354 nm. Hence, the population of $^4F_{3/2}$ arises from the continuous nonradiative population, while the $Cr^{3+} \rightarrow Nd^{3+}$ energy transfer initially populates $^4G_{9/2}$ other than $^4F_{3/2}$ under the excitation at 640 nm.
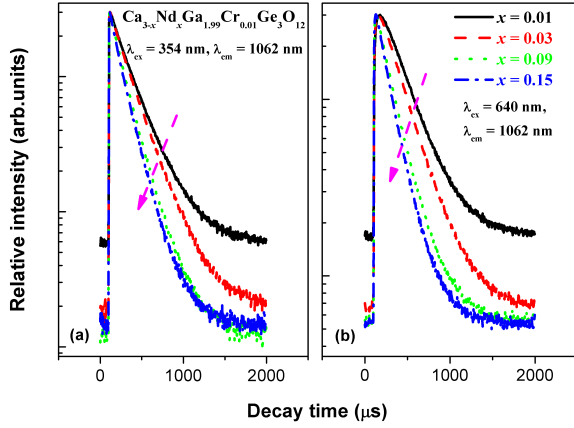
Fig. 7. (a, b)The decay curves of the samples $Ca_{3-x}Nd_xGa_{1.99}Cr_{0.01}Ge_3O_{12}$ (x = 0.01, 0.03, 0.09, 0.15) under different excitation and emission wavelengths at RT.

The increase of NIR luminescence traps of Nd³⁺ in Ca₃Ga₂Ge₃O₁₂: Nd³⁺, Cr³⁺

As discussed in the above section, the energy transfer from Cr^{3+} to Nd^{3+} is obviously occurred. However, from Fig. 6, it is found that Cr^{3+} emission decreases when increasing the Nd^{3+} concentration, while Nd^{3+} emission doesn't monotonically increase. The integral emission intensity of Nd^{3+} ion increases with the increase of Nd^{3+} concentrations (x) first, reaching a maximum value around x = 0.03, and then decreases when increasing its content (x) due to the concentration quenching. Thus the optimal concentration for Nd^{3+} ion is x = 0.03, which is consistent with a single doped Nd^{3+} concentration. Similar spectral properties occur in another group of samples $Ca_{2.97}Nd_{0.03}Ga_{2-x}Cr_xGe_3O_{12}$ (x = 0, 0.005, 0.01, 0.03, 0.05, 0.07).
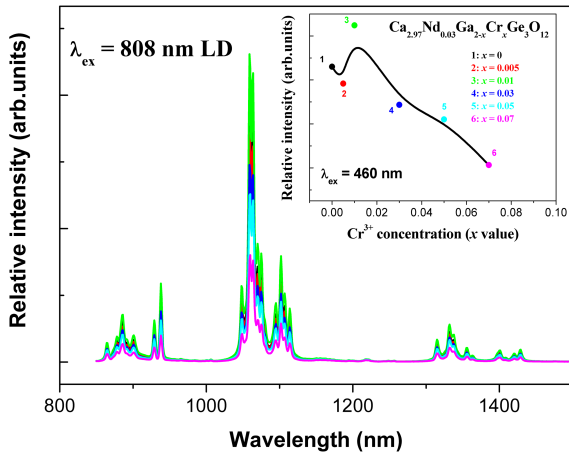
Fig. 8. The DS emission spectra of the samples $Ca_{2.97}Nd_{0.03}Ga_{2-x}Cr_xGe_3O_{12}$ upon 808 nm LD excitation with the power density of 1.05 W/cm². The inset shows the emission intensities of Nd^{3+} on the Cr^{3+} concentration under 460 nm excitation.

Fig. 8 illustrates the DS emission spectra of the samples $Ca_{2.97}Nd_{0.03}Ga_{2-x}Cr_xGe_3O_{12}$ (x = 0, 0.005, 0.01, 0.03, 0.05, 0.07) upon 808 nm LD excitation with the power density of 1.05 W/cm². One can observe the Nd^{3+} emission decreases by increasing the Cr^{3+} concentration except for x = 0.01 compared with the singly doped Nd^{3+} sample. It is possible that there are two channels of upconversion (UC) and DS when using 808 nm LD as an excitation source in CGGG: Nd^{3+}, Cr^{3+}. With

introducing the Cr^{3+} ion, it has little effect on the DS process due to without direct energy transfer from Nd^{3+}:$^4F_{5/2}$ to Cr^{3+}:$^4T_2(^4F)$, but the NIR emission intensity of Nd^{3+} is dependent on the content of Cr^{3+} ion. It indicates that the Cr^{3+} ion is involved in the UC process, where a new energy transfer path is forming to affect the de-excitation. The CGGG:Cr^{3+} samples have an absorption band spanning from 380 to 520 nm, which implies that the energy of two photons of infrared pumping laser can be simultaneously absorbed. [26] Pumping the Nd^{3+} by using focused 808 nm LD produces the population of electrons in the excited state in blue band, the excited electrons nonradiatively relax to the lowest energy state and transfer energy to Cr^{3+} by cross relaxation, and then the energy absorbed by Cr^{3+} ions is subsequently transferred to Nd^{3+} ions, leading to the characteristic DS luminescence attributed to the energy transition of Nd^{3+}. The entire energy-transfer path is by the way of $Nd^{3+}(808\,nm) \xrightarrow{UC} Cr^{3+}(460\,nm) \xrightarrow{CR} Nd^{3+}(1062\,nm)$. While UC and DS are the two competing processes by the influence of Cr^{3+} doping concentration. Therefore, with the increase in Cr^{3+} concentrations, the Nd^{3+} NIR-to-NIR DS emission basically decreases due to the two possible factors, i.e. (1) UC of Nd^{3+} and (2) the increase traps by Cr^{3+} co-doped into CGGG:Nd^{3+}, the latter will be discussed in the following content.

In order to characterize the enhancement in Nd^{3+} NIR emission, the emission spectra of $Ca_{2.97}Nd_{0.03}Ga_{2-x}Cr_xGe_3O_{12}$ samples in the range of 700-1400 nm were measured under 254, 460, 640 nm excitations, respectively. As an example, the emission intensities of Nd^{3+} versus the Cr^{3+} concentration upon 460 nm excitation is shown in the inset of Fig. 8. Similar variation of Nd^{3+} emission intensities with the increase of Cr^{3+} concentration could be observed. Optimal composition of NIR emission of Nd^{3+} in CGGG is $Ca_{2.97}Nd_{0.03}Ga_{1.99}Cr_{0.01}Ge_3O_{12}$. This means that the energy transfer from Cr^{3+} to Nd^{3+} does not enhance the Nd^{3+} emission. The contradiction could be explained as the simultaneous increase of luminescence traps. It is speculated that the increased energies are mostly captured by traps.
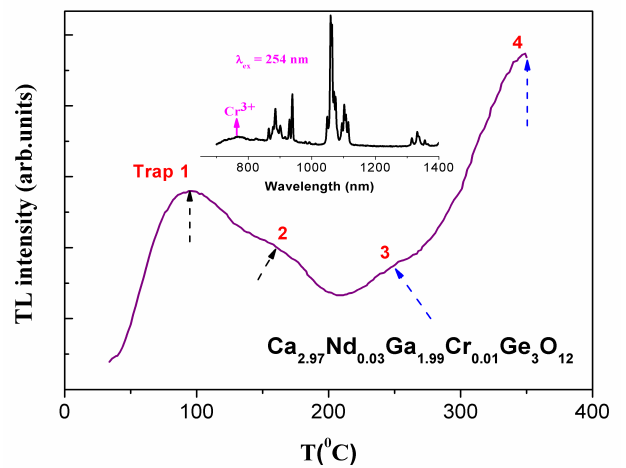

Fig. 9. TL curves of the samples $Ca_{2.97}Nd_{0.03}Ga_{1.99}Cr_{0.01}Ge_3O_{12}$ under 254 nm excitation for 5 min.

The increase in luminescence traps can be confirmed by TL measurement. Fig. 9 shows the TL curves of the samples

$Ca_{2.97}Nd_{0.03}Ga_{1.99}Cr_{0.01}Ge_3O_{12}$ after 254 nm excitation for 5 min. Considering the singly doped Cr^{3+} [ref. (10)] and Nd^{3+} (Figure 4), the traps 1 and 2 are similar with those observed in Cr^{3+}/Nd^{3+} doped samples. It is worth noting that Cr^{3+} emission at 750 nm can be neglected upon 254 nm excitation when Cr^{3+}-Nd^{3+} are co-doped in CGGG because of its very weak intensity compared to Nd^{3+} in NIR range (as shown in the inset of Figure 9). Therefore, the traps 1 and 2 in Fig. 9 could be considered to only come from Nd^{3+} in CGGG. While the other two traps 3 and 4 maybe due to the new generation of traps at CGGG: Nd^{3+} by co-doping Cr^{3+}. In general, the doped Nd^{3+} ion enters the dodecahedral site of Ca^{2+}, while transition metal Cr^{3+} ion enters the octahedral site of Ga^{3+} in the CGGG host due to the similar ionic radii. The compensation of the excess charge of the Nd^{3+} ions can be performed by Ga^{3+} ions substituting Ge^{4+} tetrahedral d-lattice ions. Thus, disorder might be introduced into the host lattice due to the possibility of forming different types of Nd^{3+} (Ca^{2+})-Ga^{3+} (Ge^{4+}) associations.[21,27]

Here, we consider that the increase of Nd^{3+} NIR luminescence traps is due to host lattice disorder by Cr^{3+} co-doped Nd^{3+} in CGGG. In fact, it is also possible that the doping of Nd^{3+} ions into CGGG: Cr^{3+} makes the TL band (CGGG: Cr^{3+}) broader, i.e., produces other deeper traps. It was reported that such additional deeper traps induced by Ln^{3+} doping can further capture and immobilize free carriers and subsequently improve LLP performance. But based on our experiment results (e.g. the emission spectrum upon 354 nm excitation or the excitation spectrum under 750 nm emission), it is found that energy back transfer from Nd^{3+} to Cr^{3+} is almost impossible, thus it is reasonable to ignore the Cr^{3+} emission in co-doped samples.

Fig. 10 shows the schematic electronic energy levels based on our measured results for Cr^{3+} and Nd^{3+} ions together with band gap and traps in the CGGG host, which can explain the above experimental phenomena. Upon 460 nm excitation, strong Nd^{3+} NIR emission and relatively weak Cr^{3+} emission were observed, as shown in Fig. 6. It is understandable that energy transfer occurs from Cr^{3+} to Nd^{3+} via cross-relaxation between $^4T_2$-$^4A_2$ of Cr^{3+} and $^4I_{9/2}$-$^4F_{5/2}$ transition of Nd^{3+}. It is likely that a cross-relaxation energy transfer path, namely Cr^{3+} $(^4T_2)$ + $Nd^{3+}(^4I_{9/2})$ →Cr^{3+} $(^4A_2)$ + $Nd^{3+}(^4F_{5/2})$ (denoted by ① step) plays an important role in the energy transfer. Additionally, another path is an excited state resonant energy transfer, denoted by ② step. The $^4T_2(^4P)$ state energy from Cr^{3+} is close to that from $^4G_{9/2}$ of Nd^{3+}, then the resonant energy transfer can readily occur. However, in this process, the transfer energy could be captured partly by the traps 3 and 4, especially trap 4. Therefore, Nd^{3+} NIR emission intensity doesn't always increase in either $Ca_{3-x}Nd_xGa_{1.99}Cr_{0.01}Ge_3O_{12}$ (x = 0.01, 0.03, 0.09, 0.15) or $Ca_{2.97}Nd_{0.03}Ga_{2-x}Cr_xGe_3O_{12}$ (x = 0.005, 0.01, 0.03, 0.05, 0.07). Since Cr^{3+} is co-doped in CGGG:Nd^{3+} leading to the increased luminescence traps, energy storing by traps and radiation emission are competing. Specifically, more capturing energy means, less radiative emission intensity, and vice versa. Gaining longer lasting phosphorescence could be achieved by increasing NIR luminescence traps through the route of co-doping Cr^{3+} into CGGG: Nd^{3+}. On the other hand, NIR-to-NIR luminescence is only associated with the Nd^{3+} ion dopants in CGGG.
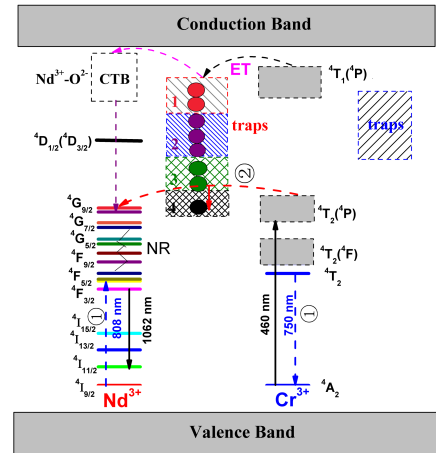

Fig. 10. Energy level diagram for Cr^{3+} and Nd^{3+} doped CGGG and possible energy transfer mechanism.

Conclusions

The NIR PL and NIR LLP of Nd^{3+} in CGGG:Nd^{3+}/Cr^{3+} phosphors have been investigated via analyzing NIR emission spectra and traps in TL curves. The results indicate that NIR LLP performance can be improved through producing the deeper traps to store more energy when co-doping Cr^{3+} into CGGG:Nd^{3+}. The energy transfer from Cr^{3+} to Nd^{3+} occurs with a high efficiency up to 57.5%. Optimal composition of NIR emission of Nd^{3+} in CGGG is $Ca_{2.97}Nd_{0.03}Ga_{1.99}Cr_{0.01}Ge_3O_{12}$. Apart from this, the NIR emission intensity ascribed to the energy transition of Nd^{3+} in co-doped samples is lower compared to the samples with single dopant, due to the generation of the deeper traps. It is interesting to find that similar phenomenon takes place upon 808 nm LD excitation, suggesting an continuous energy transfer path as $Nd^{3+}(808\,nm) \xrightarrow{UC} Cr^{3+}(460\,nm) \xrightarrow{CR} Nd^{3+}(1062\,nm)$. It is implied that NIR LLP can be achieved in Cr^{3+}-Nd^{3+} co-doped CGGG under NIR excitation at the wavelength of 808 nm. Noted that, there are still many factors, such as the different sample preparation, the luminous efficacy, initial afterglow intensity persistent duration, which would be crucial for NIR LLP to the application in vivo optical imaging.

Acknowledgements

Notes and references

1   G. Blasse and B. C. Grabmaier, *Luminescent Materials* Springer-Verlag press, Berlin, 1994, p. 65.

2   M. K. Tsang, G. X. Bai and J. H. Hao, *Chem. Soc. Rev.*, 2015, **44**, 1585.
3   T. Maldiney, A. Bessière, J. Seguin, E. Teston, S. K. Sharma, B. Viana, A. J. J. Bos, P. Dorenbos, M. Bessodes, D. Gourier, D. Scherman and C. Richard, *Nat. Mater.*, 2014, **13**, 418.
4   F. Liu, Y. J. Liang and Z. W. Pan, *Phys. Rev. Lett.*, 2014, **113**, 177401.
5   Z. J. Li, Y. W. Zhang, X. Wu, L. Huang, D. S. Li, W. Fan and G. Han, *J. Am. Chem. Soc.*, 2015, **137**, 5304.
6   Z. W. Pan, Y. Y. Lu and F. Liu, *Nat. Mater.*, 2012, **11**, 58.
7   F. Liu, W. Z. Yan, Y. J. Chuang, Z. P. Zhen, J. Xie and Z. W. Pan, *Sci. Rep.*, 2013, **3**, 1554.
8   W. Z. Yan, F. Liu, Y. Y. Lu, X. J. Wang, M. Yin and Z. W. Pan, *Opt. Express*, 2010, **18**, 20215.
9   A. Bessière, S. K. Sharma, N. Basavaraju, K. R. Priolkar, L. Binet, B. Viana, A. J. J. Bos, T. Maldiney, C. Richard, D. Scherman and D. Gourier, *Chem. Mater.*, 2014, **26**, 1365.
10 D. Q. Chen, Y. Chen, H. W. Lu and Z. G. Ji, *Inorg. Chem.*, 2014, **53**, 8638.
11 S. K. Sharma, A. Bessière, N. Basavaraju, K. R. Priolkar, L. Binet, B. Viana and D. Gourier, *J. Lumin.*, 2014, **155**, 251.
12 S. K. Sharma, D. Gourier, B. Viana, T. Maldiney, E. Teston, D. Scherman and C. Richard, *Opt. Mater.*, 2014, **36**, 1901.
13 Y. X. Zhuang, J. Ueda, S. Tanabe and P. Dorenbos, *J. Mater. Chem. C*, 2014, **2**, 5502.
14 Y. Li, Y. Y. Li, R. C. Chen, K. Sharafudeen, S. F. Zhou, M. Gecevicius, H. H. Wang, G. P. Dong, Y. L. Wu, X. X. Qin and J. R. Qiu, *NPG Asia Mater.*, 2015, **7**, e180.
15 C. Y. Liu, Z. G. Xia, M. S. Molokeev and Q. L. Liu, *J. Am. Ceram. Soc.*, 2015, **98**, 1870.
16 J. P. Shi, X. Sun, J. L. Li, H. Z. Man, J. S. Shen, Y. K. Yu and H. W. Zhang, *Biomaterials*, 2015, **37**, 260.
17 E. Teston, S. Richard, T. Maldiney, N. LiÀvre, Guillaume. Y. Wang, L. Motte, C. Richard and Y. Lalatonne, *Chem. Eur. J.*, 2015, **21**, 7350.
18 S. Kamimura, C. N. Xu, H. Yamada, N. Terasaki, and M. Fujihala, *Jpn. J. Appl. Phys.*, 2014, **53**, 092403.
19 J. Ueda, T. Shinoda and S. Tanabe, *Opt. Mater. Express*, 2013, **3**, 787.
20 Y. Teng, J. J. Zhou, Z. J. Ma, M. M. Smedskjaer and J. R. Qiu, *J. Electrochem. Soc.*, 2011, **158**, K17.
21 U. Caldifio G.; M. Voda, F. Jaque, J. G. Sole and A. A. Kaminskii, *Chem. Phys. Lett.*, 1993, **213**, 84.
22 V. Kumar, S. Kr. Sharma, T. P. Sharma and V. Singh, *Opt. Mater.*, 1999, **12**, 115.
23 S. L. Dong, H. H. Lin, T. Yu and Q. Y. Zhang, *J. Appl. Phys.*, 2014, **116**, 023517.
24 F. T. You, A. J. J. Bos, Q. F. Shi, S. H. Huang and P. Dorenbos, *Phys. Rev. B*, 2012, **85**, 115101.
25 A. J. J. Bos, R. M. van Duijvenvoorde, E. van der Kolk, W. Drozdowski and P. Dorenbos, *J. Lumin.*, 2011, **131**, 1465.
26 L. Y. Yang, Y. J. Dong, D. P. Chen, C. Wang, N. Da, X. W. Jiang, C. H. Zhu and J. R. Qiu, *Opt. Express*, 2005, **13**, 7893.
27 K. Korthout, K. Van den Eeckhout, J. Botterman, S. Nikitenko, D. Poelman and P. F. Smet, *Phys. Rev. B*, 2011, **84**, 085140.